Journal of Materials Chemistry A

ROYAL SOCIETY OF CHEMISTRY

PAPER

View Article Online
View Journal | View Issue

Cite this: J. Mater. Chem. A, 2021, 9, 6252

Solar-driven valorisation of glycerol on $BiVO_4$ photoanodes: effect of co-catalyst and reaction media on reaction selectivity†

Yi-Hsuan Wu, [a] Denis A. Kuznetsov, *[a] Nicholas C. Pflug, [b] Alexey Fedorov [a] and Christoph R. Müller *[a]

The electrochemical valorization of glycerol, a by-product from biodiesel production, has received significant attention, yet systems for the efficient reforming of glycerol that are based on non-precious metals have rarely been reported. Here, we introduce tungsten-doped bismuth vanadate (W:$BiVO_4$) electrodes combined with an atomic-layer-deposited nickel (oxy)hydroxide ($NiO_x(OH)_y$) co-catalyst, as a promising photoanode material for the photoelectrochemical (PEC) oxidation of glycerol. To reveal trends in the reaction kinetics and selectivities, glycerol oxidation reaction (GOR) was investigated in varying electrolytes and at different applied biases. The photoanode developed in our study provides a rare example of the efficient production of the high value-added products, dihydroxyacetone (DHA), glyceraldehyde (GALD), and glycolaldehyde (GCALD), in the absence of precious metal catalysts. Under optimized conditions, W:$BiVO_4$ with a $NiO_x(OH)_y$ co-catalyst features oxidation currents and onset potentials for glycerol/water oxidation that are on par with state-of-the-art transition-metal-oxide photoanodes employed for the reforming of organic species, which marks an important step towards affordable solar-driven electrolyzers and direct alcohol fuel cells.

Received 27th October 2020
Accepted 4th February 2021

DOI: 10.1039/d0ta10480a

rsc.li/materials-a

Introduction

Molecular hydrogen H_2 is a promising energy carrier, which can be used directly in emission-free fuel cell devices,[1–3] or in hydrogenation reactions to produce high-energy-density chemicals such as ammonia[4,5] or methanol.[6–8] Conventionally, hydrogen is produced by the reforming of fossil fuels thus contributing appreciably to industrial CO_2 emissions.[9] Electrolysis of water[10] offers a potentially sustainable alternative way for H_2 synthesis, if coupled with renewable electricity sources such as wind, hydropower or sunlight-driven photovoltaics.[11,12] Complementing water splitting, the (photo)electrochemical oxidation of cheap and abundant organics or biomass feedstocks (*e.g.* glycerol) is an emerging field with enormous potential for the production of hydrogen and value added chemicals.[13,14] While the splitting of water into H_2 and O_2 is highly endothermic ($\Delta G^\circ = 237$ kJ mol^{-1}), requiring a minimum cell voltage of $\Delta E^\circ = 1.23$ V,[12] supplemented by the reaction overpotential (typically >0.5 V to achieve industrially relevant current densities), the dehydrogenative reforming of abundant carbohydrates or alcohols requires a relatively low external energy input.[15] Moreover, the products of the partial oxidation of organic feedstocks can be of high market value (for instance, dihydroxyacetone is used in the cosmetics industry).[16] Yet the highly efficient catalysts composed of abundant elements for the reforming of organic species are not developed, in part as a result of a limited fundamental understanding of the reaction pathways of the organics valorisation to selectively produce H_2 and valuable oxygenates.

The use of semiconductor electrodes in a photoelectrochemical (PEC) setup allows to reduce considerably the reaction overpotentials, paving the way towards unbiased solar-driven photocatalysis.[17,18] Bismuth vanadate ($BiVO_4$) has been identified as one of the most promising photoanodes, exploited initially for water splitting.[19] In the monoclinic phase, $BiVO_4$ is the photoactive n-type semiconductor with a bandgap of 2.4 eV,[20,21] *i.e.* it absorbs in the visible light range. However, unmodified $BiVO_4$ features low catalytic activity for photoelectrochemical water oxidation. To enhance kinetics, improve charge transport characteristics and reduce surface recombination of the photo-generated charge carriers in $BiVO_4$, different strategies have been employed, *i.e.* aliovalent doping or deposition of co-catalysts for the oxygen evolution reaction.[22] As a result, the range of application for $BiVO_4$-based photocatalysts expanded from water oxidation[20] to other photo(electro)catalytic transformations, such as the oxidation of 5-hydroxymethylfurfural, degradation of organic dyes or CO_2

[a]Department of Mechanical and Process Engineering, ETH Zürich, Leonhardstrasse 21, 8092 Zürich, Switzerland. E-mail: denisk@ethz.ch; muelchri@ethz.ch

[b]Department of Environmental Systems Science, ETH Zürich, Universitätstrasse 16, 8092 Zurich, Switzerland

† Electronic supplementary information (ESI) available. See DOI: 10.1039/d0ta10480a

conversion.[23–25] Despite these advances, $BiVO_4$ remains underutilized for the reforming of abundant organic feedstock molecules to H_2 and partially-oxidized value-added organic chemicals.

In the present study, we evaluate the performance of $BiVO_4$-based photoanodes for the photoelectrocatalytic reforming of glycerol, $C_3H_5(OH)_3$. Glycerol, a side product of biodiesel production, is a highly abundant and inexpensive chemical[26] formed during the transesterification of triglycerides with methanol (one mole of glycerol is generated per three moles of biodiesel,[27] which corresponds to *ca.* 100 kg of glycerol produced per ton of biodiesel). Oxidation, or the partial dehydrogenative reforming of glycerol, can in principle generate a plethora of the high value-added chemicals, *e.g.* 1,3-dihydroxyacetone, glyceraldehyde, tartronic acid, glycolic acid or hydroxypyruvic acid (Scheme 1).[28] On the other hand, the complete dehydrogenative decomposition of one mole of glycerol can generate up to four moles of hydrogen at a relatively low energy input ($\Delta G = 3.9$ kJ $mol_{glycerol}^{-1}$).[16] Therefore, glycerol has a potential to be used in both H_2 generating electrolyzers and direct alcohol fuel cells.[29,30]

Here, we present the study of the photoelectrochemical glycerol oxidation on $BiVO_4$-based photoanodes in different pH environments. Our work demonstrates that tungsten doping in the $BiVO_4$ structure, aided by the deposition of a nickel oxyhydroxide (denoted in the text as $NiO_x(OH)_y$, see discussion below) co-catalyst layer, notably improves the kinetics of glycerol oxidation on the photoanode. We focused on the development and optimization of the nickel-based coatings as the latter demonstrated promising electro- and photoelectrocatalytic activity and stability in a related reaction of water oxidation[31,32] as well as in electrocatalytic glycerol oxidation.[33] In addition, the pH of the reaction media substantially affects the distribution of products, *e.g.* formation of glyceraldehyde (GALD) is only observed in acidic conditions. Glycolaldehyde (GCALD), the simplest α-hydroxycarbonyl synthon for sugar formation, to the best of our knowledge, was for the first time observed in PEC glycerol oxidation. Our study clarifies the effects of different reaction variables (*e.g.* pH, applied bias, presence of co-catalysts) on the kinetics of PEC glycerol reforming. Thus, tungsten-doped bismuth vanadate (W:$BiVO_4$) with an atomic-layer-deposited $NiO_x(OH)_y$ co-catalyst achieved a photocurrent of 4.2 mA cm^{-2} at 1.2 V_{RHE} (0.5 M Na_2SO_4), which is on par with the most active photocatalysts employed to date for the decomposition of organic substrates and biomass derivatives.[34] Overall, our approach represents an effective, scalable strategy for producing solar hydrogen and offers a pathway to valorise abundant low cost glycerol.

Results and discussion

Materials synthesis and characterization

Electrodes containing W-doped $BiVO_4$ films on fluorine doped tin oxide (FTO) coated glass substrates were fabricated by a general electrodeposition-calcination method,[34–36] modified slightly in this work (details are given in ESI†). The tungsten dopant was introduced into $BiVO_4$ during a calcination step in order to enhance the bulk charge transfer efficiency of the material[37] (denoted W:$BiVO_4$; W content is 0.5 at% according to ICP, Fig. S1†). Nickel-based coating was deposited onto W:$BiVO_4$-based electrodes *via* atomic layer deposition (ALD)[38] using pulses of nickelocene ($Ni(\eta^5\text{-}C_5H_5)_2$, $NiCp_2$) and H_2O at 250 °C (see ESI† for detailed experimental procedures). Nickel-coated W:$BiVO_4$ electrodes (Ni content of 0.65 at%) were used for PEC measurements without further thermal treatment.

X-ray diffraction (XRD) pattern of as-synthesized W:$BiVO_4$ matches that of a monoclinic scheelite reference (no. 01-083-1699, ICDD database, Fig. 1a). W:$BiVO_4$ has a porous structure according to scanning electron microscopy imaging (SEM, Fig. S2†). No additional peaks were observed in the diffraction pattern of W:$BiVO_4$, after atomic-layer-deposition of nickel coating (Fig. 1a).

Nickel-coated W:$BiVO_4$ electrodes were subjected to five anodic scans, from −0.05 to 1.50 V_{RHE} in 0.5 M potassium borate buffer solution (KB_i, pH = 9.3) (Fig. S3a†), and then used for glycerol oxidation. Such electrochemical activation yields $NiO_x(OH)_y$ species in the form of uniformly distributed crystalline nanoparticles on the surface of W:$BiVO_4$, according to high-resolution transmission electron microscopy (HRTEM), high-angle annular dark-field scanning transmission electron microscopy (HAADF-STEM) and energy dispersive X-ray spectroscopy (EDX) elemental mapping (Fig. 1b). XRD of anodically-activated $NiO_x(OH)_y$/W:$BiVO_4$ electrodes is identical to that of

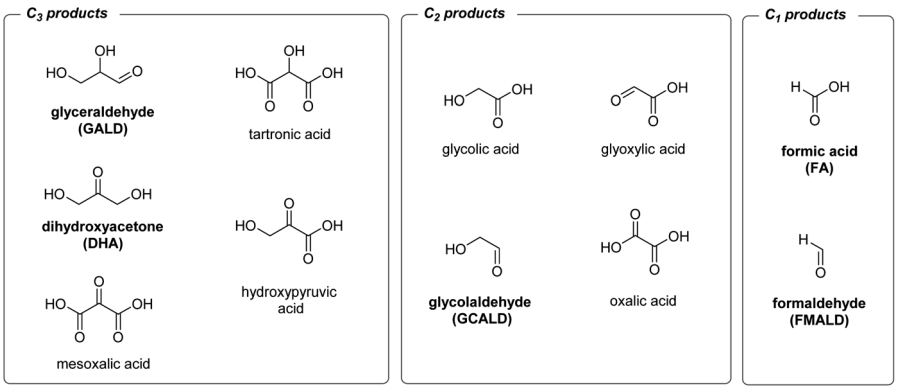

Scheme 1 Products of electrochemical glycerol reforming identified in the literature. Products found in this study are shown in bold.

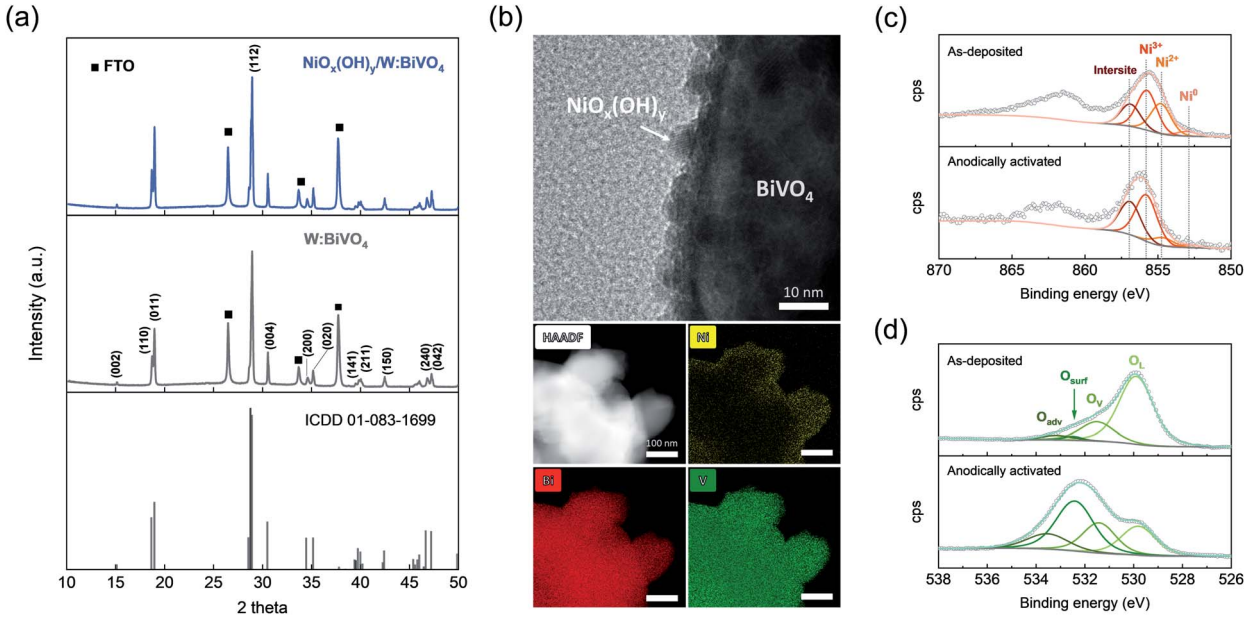

Fig. 1 (a) XRD patterns of $BiVO_4$ (ICDD no. 01-083-1699), W:$BiVO_4$ and as-deposited $NiO_x(OH)_y$/W:$BiVO_4$. The peaks corresponding to the FTO substrate are indicated by squares. (b) HRTEM, HAADF-STEM, and EDX elemental mapping images of electrochemically activated $NiO_x(OH)_y$/W:$BiVO_4$ electrodes. Overlay of the (c) Ni 2p and (d) O 1s core level XPS signals of as-deposited and electrochemically activated $NiO_x(OH)_y$/W:$BiVO_4$. The feature denoted as intersite (856.9 eV) is due to defects in the structure, as discussed elsewhere.[39]

the as prepared $NiO_x(OH)_y$/W:$BiVO_4$ (Fig. S3b†). A negligible difference in the absorption spectra of $NiO_x(OH)_y$/W:$BiVO_4$ and W:$BiVO_4$ indicates that ALD-deposited $NiO_x(OH)_y$ does not alter noticeably light absorption properties of the photoanode (Fig. S3c†).

The surface composition and valence states of as-deposited and anodically activated $NiO_x(OH)_y$/W:$BiVO_4$ were probed by X-ray photoelectron spectroscopy (XPS). The Ni 2p core level XPS spectrum of as-deposited $NiO_x(OH)_y$/W:$BiVO_4$ reveals features ascribed to metallic Ni, Ni^{2+} and Ni^{3+} at 852.9, 854.7 and 855.7 eV, respectively, while an additional feature at higher binding energy (denoted as intersite, 856.9 eV) can be ascribed to the presence of defects in the nickel (oxy)hydroxide structure (Fig. 1c).[39] As expected, anodic activation increased the relative amount of oxidized nickel species ($NiO_x(OH)_y$), evidenced by the much enhanced intensity of the feature at 855.7 eV.

The O 1s core level spectrum (Fig. 1d) of as-deposited and activated $NiO_x(OH)_y$/W:$BiVO_4$ films can be deconvoluted into four components: lattice oxygen (O_L, 529.5 eV), lattice oxygen sites located in the vicinity of oxygen vacancies/defects (O_V, 531 eV), surface oxygen species (O_{surf}, 532 eV), and adventitious species (weakly bound adsorbed water/CO_2, O_{adv}).[40,41] Comparison of the spectra of the as-deposited and activated films reveals a distinct increase in the concentration of surface oxygen groups for the electrochemically activated films, *i.e.* an increase from 2 to 42%, consistent with the formation of layered nickel oxyhydroxide species with a highly exposed surface (Table S1†).[42]

Photoelectrochemical oxidation of glycerol

To investigate the performance of the electrochemically activated $NiO_x(OH)_y$/W:$BiVO_4$ electrodes (see above) for PEC glycerol oxidation, photoelectrochemical studies were carried out using a custom-made, two-compartment cell with an anion-exchange membrane. Glycerol oxidation was studied in mild alkaline media (0.5 M potassium borate buffer, KB_i, pH = 9.3) and in non-buffered electrolyte (0.5 M Na_2SO_4, pH = 7.0), which gradually acidifies during the PEC reaction. In the following sections, we discuss the photoelectrochemical activity of the fabricated materials for glycerol oxidation, their long-term stability for GOR, and the distribution of the reaction products as a function of the reaction conditions (electrolyte, applied bias).

Fig. 2a and b show the linear sweep voltammetry (LSV) profiles under dark and illumination conditions for W:$BiVO_4$ and $NiO_x(OH)_y$/W:$BiVO_4$ in 0.5 M KB_i and 0.5 M Na_2SO_4 electrolytes. In Na_2SO_4 solution, the PEC performance of W:$BiVO_4$ is characterized by an onset potential of *ca.* 0.43 V_{RHE} and a photocurrent for water oxidation of 2.3 mA cm^{-2} at 1.2 V_{RHE} (in the absence of glycerol). The $NiO_x(OH)_y$ co-catalyst enhances the photocurrent to 3.3 mA cm^{-2} (1.2 V_{RHE}), leading to a *ca.* 50 mV cathodic shift of the onset potential. In the presence of glycerol (0.1 M), the photocurrent increases in the entire potential range, reaching 4.2 mA cm^{-2} at 1.2 V_{RHE}.

In mild-alkaline conditions (0.5 M KB_i), W:$BiVO_4$ and $NiO_x(OH)_y$/W:$BiVO_4$ exhibit *ca.* 50 mV cathodic shift of the onset potential on the RHE scale relative to that in the Na_2SO_4 electrolyte (Fig. 2b). The photocurrent for glycerol oxidation on $NiO_x(OH)_y$/W:$BiVO_4$ electrodes reaches 2.5 mA cm^{-2} (0.8 V_{RHE}) and increases to 3.5 mA cm^{-2} at 1.2 V_{RHE}, thus matching or exceeding the performance of some transition-metal-oxide-based PEC systems (*e.g.* TiO_2) employed for the oxidation of organic alcohols (methanol, ethanol or glycerol).[34] Control

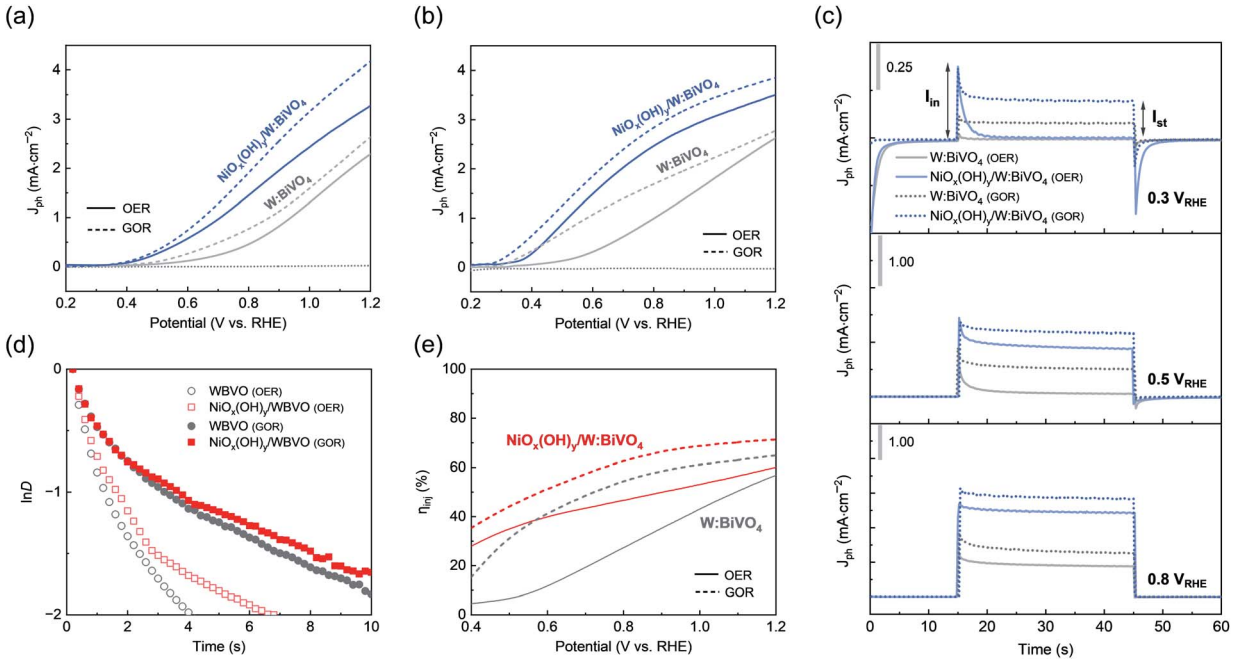

Fig. 2 Linear sweep voltammetry of W:$BiVO_4$ and $NiO_x(OH)_y$/W:$BiVO_4$ in (a) 0.5 M Na_2SO_4 and (b) 0.5 M KB_i with and without the addition of 0.1 M glycerol under dark and AM 1.5 G, 100 mW cm^{-2} illumination; scan rate = 10 mV s^{-1}. (c) Chopped chronoamperometry plots of W:$BiVO_4$ and $NiO_x(OH)_y$/W:$BiVO_4$ in 0.5 M KB_i with (dotted lines) and without (solid lines) 0.1 M glycerol at 0.3 V_{RHE}, 0.5 V_{RHE}, and 0.8 V_{RHE}. The color code is the same as on panels a and b. (d) Plots of ln D as a function of time of photoanodes for water oxidation and glycerol oxidation (E = 0.5 V_{RHE}). (e) Hole injection efficiency *vs.* applied bias for glycerol oxidation in 0.5 M KB_i; the corresponding linear sweep voltammetry of sulfite oxidation is presented in the ESI.†

experiments show a high reproducibility of the data collected on W:$BiVO_4$ and $NiO_x(OH)_y$/W:$BiVO_4$ photoelectrodes (Fig. S3d†). Overall, the enhancement of the catalytic activity of $NiO_x(OH)_y$/W:$BiVO_4$ for water and glycerol oxidation in mildly alkaline conditions relative to neutral conditions may originate from the pH-dependence of the electrocatalytic activity of the $NiO_x(OH)_y$ co-catalyst layer, which is a typically observed phenomenon for nickel or cobalt-based oxides and (oxy) hydroxides.[43,44]

The charge-transfer dynamics at the semiconductor–electrolyte interface (SEI) was analysed by the transient photocurrent profile at a constant potential. Here, we used alkaline 0.5 M KB_i conditions and relatively low biases, *i.e.* 0.3 V_{RHE}, 0.5 V_{RHE}, and 0.8 V_{RHE} (Fig. 2c). The initial transient photocurrent, I_{in}, is caused by the separation of the photogenerated hole–electron pairs, where trapping or recombination of charge carriers takes place by surface states or reduced species in an electrolyte.[45] The continuous decay of the photocurrent indicates ongoing recombination until a steady state, I_{st}, is reached. When the light is off, back-reaction of electrons at the conduction band with accumulated holes results in a negative current spike.

In the absence of glycerol, the steady-state photocurrent at 0.3 V_{RHE} (*i.e.* close to the onset potential) is nearly zero for W:$BiVO_4$ and $NiO_x(OH)_y$/W:$BiVO_4$ electrodes, coinciding with the onset potential observed in the LSV profile. In the presence of glycerol, a distinct non-zero photocurrent is detected reaching 80 μA cm^{-2} (0.3 V_{RHE}), 0.53 mA cm^{-2} (0.5 V_{RHE}) and 1.22 mA cm^{-2} (0.8 V_{RHE}) for the W:$BiVO_4$ electrodes (Fig. 2c). In addition, the back-reaction current was significantly suppressed at 0.3 V_{RHE}, likely indicating a reduced accumulation of holes at the material surface. In the presence of glycerol, the photocurrent of the $NiO_x(OH)_y$/W:$BiVO_4$ electrodes increased to 0.2 mA cm^{-2} (0.3 V_{RHE}), 1.2 mA cm^{-2} (0.5 V_{RHE}) and 2.9 mA cm^{-2} (0.8 V_{RHE}). Note that all the studied potentials are below the thermodynamic potential of the water oxidation, 1.23 V_{RHE}.

The photocurrent relaxation dynamics were also analysed using the transient decay time τ, expressed by a logarithmic plot of the parameter D (eqn (1)) *versus* time, where I_t is the current at time t.[45]

$$D = \frac{I_t - I_{st}}{I_{in} - I_{st}} \quad (1)$$

The transient decay time is defined as time at which ln D = −1. The value of τ reflects the electron lifetime within bulk semiconductor. $BiVO_4$ is known to undergo facile recombination of charge carriers due to sluggish charge-transfer kinetics at the SEI.[46] Since the accumulated holes at the surface facilitate electron–hole recombination leading to a reduced lifetime of the separated charges, a facilitated hole transfer to the reagents in the electrolyte will prolong the lifetime of the separated electrons. At 0.5 V_{RHE}, W:$BiVO_4$ suffers from severe surface recombination, resulting in τ of *ca.* 1.3 s. Upon addition of glycerol acting as a hole acceptor, an enhanced charge transport from the near-surface region to the electrolyte gives rise to

a near three-fold enhancement of τ reaching 4.0 s (Fig. 2d). Overall, these observations of an increased photocurrent and a longer transient decay time imply faster kinetics of the photoelectrochemical glycerol oxidation reaction as compared to the oxygen evolution reaction (OER) in water.

The analysis of the hole-injection efficiency (η_{inj}, see ESI and Fig. S4 for details†) for glycerol oxidation on the studied photoanodes further corroborates this conclusion. The sulfite anion (SO_3^{2-}) is a typically used hole scavenger, whose η_{inj} can be taken as a reference value (100%).[47] The hole injection efficiency for water oxidation reaches *ca.* 55% and 60% on W:$BiVO_4$ and $NiO_x(OH)_y$/W:$BiVO_4$ electrodes, respectively, at 1.2 V_{RHE} (Fig. 2e). In the presence of glycerol (0.1 M), $NiO_x(OH)_y$/W:$BiVO_4$ photoelectrode exhibits a superior hole transfer to glycerol than W:$BiVO_4$ throughout the whole potential window, reaching an efficiency of 72% at 1.2 V_{RHE}, that confirms the enhancement of the kinetics of glycerol oxidation with respect to OER.

Long-term photoelectrochemical oxidation of glycerol

Two static potentials, 0.8 and 1.2 V_{RHE}, were used to investigate the effect of the applied bias on the kinetics of glycerol reforming under constant potential electrolysis conditions. Fig. S5† demonstrates 10 h chronoamperometry tests under illumination at 1.2 V_{RHE} in 0.5 M Na_2SO_4 or 0.5 M KB_i, both in the presence of 0.1 M glycerol or in a glycerol-free electrolyte. Anodic photocorrosion, *i.e.* oxidation during OER under illumination, was reported previously for $BiVO_4$ (ref. 48) and indeed, a rapid decay of the photocurrent in 0.5 M Na_2SO_4 and 0.5 M KB_i is observed for W:$BiVO_4$ electrodes (Fig. S5†). After 5 h of electrolysis, merely 26% and 20% of the photoactivity is retained in 0.5 M Na_2SO_4 and 0.5 M KB_i, respectively. In contrast, in the presence of glycerol, an excellent stability along with a marked increase of the current was observed, likely indicative of the preferential oxidation of glycerol over water on the W:$BiVO_4$ photoanode (Fig. S5†). Noteworthy, for the 0.5 M Na_2SO_4 electrolyte, a decrease in the pH in the anodic compartment to <3 was detected, whereas the pH remains unchanged in a 0.5 M KB_i buffer solution.

While the excellent stability of the W:$BiVO_4$ electrodes in the presence of glycerol is observed at both low (0.8 V_{RHE}) and high (1.2 V_{RHE}) biases, the degradation of $NiO_x(OH)_y$/W:$BiVO_4$ electrodes in 0.5 M KB_i takes place, as the loss of 21% (0.8 V_{RHE}) and 33% (1.2 V_{RHE}) in the photocurrent after 10 h is observed (Fig. S6†). We attribute this decrease to a gradual dissolution of the nickel catalyst, however the poisoning of the surface by adsorbed reaction intermediates or by-products can also take place.[49,50] Notably, in the absence of glycerol, the photoelectrochemical stability of $NiO_x(OH)_y$/W:$BiVO_4$ in 0.5 M KB_i is substantially higher (Fig. S7†). Inductively coupled plasma optical emission spectrometry (ICP-OES) was used to analyse the electrolyte composition after the reaction under various conditions (Fig. S8†). In the presence of glycerol, we observed a negligible dissolution of Bi and V into the electrolyte ($\leq$0.6% of the total loading) from W:$BiVO_4$ electrodes in 0.5 M KB_i, while somewhat higher values (*e.g.* $\geq$6% loss of Bi and V after continuous GOR at 1.2 V_{RHE}) are observed in 0.5 M Na_2SO_4. In contrast to bismuth vanadate, the $NiO_x(OH)_y$ overlayer proved to be unstable under the reaction conditions, *e.g.* 10 h of continuous electrolysis in 0.5 M KB_i resulted in a loss of >90% of the nickel content. However, in 0.5 M Na_2SO_4, the rate of nickel dissolution decreases significantly, *i.e.* to 35% (0.8 V_{RHE}) and 24% (1.2 V_{RHE}) after 10 h of electrolysis. XPS analysis on $NiO_x(OH)_y$/$BiVO_4$ electrode revealed absence of the noticeable changes of the chemical states of nickel after GOR in Na_2SO_4 (Fig. S9†).

HRTEM imaging of the electrodes after 10 h of glycerol oxidation in 0.5 M KB_i (Fig. S10†) confirms that $BiVO_4$ maintains its original morphology. Consistent with ICP data, the used $NiO_x(OH)_y$/W:$BiVO_4$ electrodes reveal no detectable amounts of nickel on the surface after the PEC test. Thus, the dissolution of the nickel co-catalyst layer coincides with a decrease of the photocurrent during constant potential electrolysis, serving as an indirect evidence for the crucial role of nickel surface species in catalysing glycerol oxidation on the photoanode (Fig. S6†).

To summarize, atomic-layer-deposited $NiO_x(OH)_y$ enhances the OER kinetics of W:$BiVO_4$ as reflected by an increased photocurrent and transient decay time. In the presence of glycerol, both W:$BiVO_4$ and $NiO_x(OH)_y$/W:$BiVO_4$ exhibit a high activity towards glycerol oxidation. $NiO_x(OH)_y$/W:$BiVO_4$ electrodes demonstrate appreciable photoelectrochemical stability under PEC glycerol oxidation conditions, although the gradual dissolution of the nickel cocatalyst was observed in the presence of glycerol that resulted in a continuous decay of the catalytic currents for $NiO_x(OH)_y$/W:$BiVO_4$ electrodes over time in alkaline condition. An increase of the current despite the dissolution of the $NiO_x(OH)_y$ layer during photoelectrolysis in a Na_2SO_4 solution can be attributed to the gradual acidification of the medium, which can have a positive effect on the reaction kinetics.

Product analysis: influence of electrolyte, applied bias, and $NiO_x(OH)_y$ co-catalyst on the chemoselectivity of GOR

Next, the C_1–C_3 products of glycerol oxidation during long-term GOR conditions (10 h) over W:$BiVO_4$ and $NiO_x(OH)_y$/W:$BiVO_4$ electrodes were identified and quantified by ^{1}H and ^{13}C NMR spectroscopy and high performance liquid chromatography (HPLC).

^{1}H and ^{13}C NMR spectroscopy

Previous reports have identified 1,3-dihydroxyacetone (DHA), glyceraldehyde (GALD), glyceric acid (GLA), hydroxypyruvic acid (HyP), tartronic acid (TA), glycolic acid (GLC), glyoxylic acid (GLX), oxalic acid (OA), formic acid (FA), and carbonate, CO_3^{2-}, as possible products of the (photo)electrochemical oxidation of glycerol (Scheme 1).[28,51] ^{1}H and ^{13}C NMR data acquired in our study under different PEC conditions are shown in Fig. S11, S12 and Table S2.† Note that to account for the possible photochemical degradation, the NMR spectra of glycerol discussed here are recorded from a glycerol solution exposed to AM 1.5 G, 100 mW cm^{-2} illumination for 10 h without applied bias.

0.5 M Na_2SO_4 electrolyte

In 0.5 M Na_2SO_4, GALD, GCALD, DHA, FA, and FMALD (predominantly hydrated) were detected by ^{1}H and ^{13}C NMR by comparing with standards and literature data[52] (Fig. S11, S13a and S14a†). Noteworthy, illumination of a glycerol solution (0.5 M Na_2SO_4) without applying a bias did not lead to formation of the new species, as evidenced by NMR analysis, which is indicative of a high stability of glycerol towards spontaneous photo-oxidation in Na_2SO_4 electrolyte (Fig. S11a†).

^{1}H and ^{13}C spectra collected for the $NiO_x(OH)_y$/W:$BiVO_4$ electrode at 1.2 V_{RHE} in 0.5 M Na_2SO_4 exhibit complex patterns (δ_H ~3.5–4.5 ppm and δ_C ~60–100 ppm) (Fig. S11a and b†), in which new signatures in addition to the previously identified peaks of GCALD, GALD, and DHA are found. Presumably, these signatures are due to oxygenated species that we are currently unable to identify. Previous studies have shown that GCALD, GALD, and DHA form complex equilibria of monomers and oligomers in aqueous solutions.[53–55] Analysis of the ^{1}H NMR spectrum of the product mixture obtained for the $NiO_x(OH)_y$/W:$BiVO_4$ photoanode at 1.2 V_{RHE} assumes a presence of GCALD, GALD, and DHA (by matching with the signals of the respective reference chemicals, Fig. S14†), however ^{13}C NMR of the same solutions (Fig. S11b†) showed that GCALD, GALD, and DHA do not account for all of the signals. A ^{1}H–^{1}H Correlation Spectroscopy (COSY) analysis for this mixture showed many overlapping signals making its interpretation difficult, and heteronuclear single quantum coherence spectroscopy (HSQC) (Fig. S15†) and heteronuclear multiple bond correlation (HMBC) analysis failed to show correlations for the ^{1}H signals of interest. Thus, further work is necessary to identify the as yet undetermined specie(s).

0.5 M KB_i electrolyte

Unlike with 0.5 M Na_2SO_4 electrolyte, as yet unidentified products of spontaneous glycerol decomposition under illumination were observed in a 0.5 M KB_i buffer solution, as evidenced by the appearance of noise level signals at δ_H = 2.09, 2.72, 2.91 and 3.07 ppm in the ^{1}H NMR spectra (Fig. S12a†). The product mixture contains GCALD, along with FA and FMALD, and each of these species are observed for all electrode materials tested ($NiO_x(OH)_y$/W:$BiVO_4$ and W:$BiVO_4$) and at both electrolysis potentials studied. The presence of GALD cannot, however, be ruled out, as the GALD signals overlap with those of GCALD. Notably, DHA was found in the product mixture for $NiO_x(OH)_y$/W:$BiVO_4$ electrodes, but not on bare W:$BiVO_4$ without a nickel co-catalyst (Fig. S12a, S14b and S16†). Note that no carbonate was detected in the reaction mixture as followed from the absence of the corresponding signals in ^{13}C NMR spectra (δ = 166–168 ppm).[56]

Quantitative analysis and mechanistic hypothesis

Following the identification of the key products by NMR spectroscopy, HPLC analysis of the reaction mixture was carried out to obtain quantitative information about the products formed after 5 h and 10 h of continuous photoelectrolysis under varying conditions (Fig. S17†). In general, the analysis of the products by HPLC is consistent with results of NMR spectroscopy. In 0.5 M Na_2SO_4, GALD and GCALD are identified as products by the direct comparison of retention times with commercial references measured in the same electrolyte (Fig. S17a†). In the case of glycerol oxidation in a 0.5 M KB_i buffer (pH = 9.3), GCALD is found under all experimental conditions (Fig. S17b†). Further analysis of the HPLC data is complicated by the overlap of the glycerol signal with the signals of some of the reaction products. In both electrolytes, due to the overlap of the chromatogram peaks of FMALD with those of glycerol and the overlap of the FMALD ^{1}H NMR chemical shifts with that of water, quantification of FMALD could not be performed, therefore FMALD is excluded from the discussion below.

The effect of the $NiO_x(OH)_y$ co-catalyst layer and the applied bias on the production rate (R) and faradaic efficiency (FE) of the detected products of the glycerol oxidation is illustrated in Fig. 3, based on ^{1}H NMR spectra and chromatography results. The distribution of the products of the electrolysis reaction depends on the applied potential, type of electrolyte and the electrode material (Table 1 and S19†). Specifically, in the 0.5 M Na_2SO_4, the average production rate of DHA, GALD, GCALD and FA increases with increasing potential when using the W:$BiVO_4$ electrode (Fig. 3a). At 0.8 V_{RHE}, FA is a primary product of glycerol oxidation on W:$BiVO_4$ electrodes with a FE of over 70% and a production rate of *ca.* 54 mmol h^{-1} m^{-2}, while at the higher potential of 1.2 V_{RHE}, a four-fold and five-fold enhancement of the production rate of DHA (70 mmol h^{-1} m^{-2}) and GCALD (*ca.* 60 mmol h^{-1} m^{-2}), corresponding to FE's of 19% and 11%, is observed.

For both 0.5 M Na_2SO_4 and 0.5 M KB_i electrolytes, the deposition of a $NiO_x(OH)_y$ co-catalyst layer results in an enhanced catalytic glycerol oxidation reflected in the higher photocurrents (higher total charge transfer) and product yields. For instance, at an electrolysis potential of 1.2 V_{RHE} in 0.5 M Na_2SO_4, *ca.* two-fold increase of the photocurrent was achieved upon deposition of a $NiO_x(OH)_y$ co-catalyst. In addition, an increase in the applied bias increases the production rate of the value-added DHA in the presence of $NiO_x(OH)_y$. Specifically, in 0.5 M KB_i, a three-fold enhancement of production rate of DHA (138 mmol h^{-1} m^{-2}) was achieved at 1.2 V_{RHE} (compared to 0.8 V_{RHE}) along with an improved FE of 19% (Fig. 3b and d).

Product analysis and identification enabled the proposal of reaction path(s) for the photoelectrocatalytic glycerol decomposition using W:$BiVO_4$ and $NiO_x(OH)_y$/W:$BiVO_4$ electrodes. It is proposed that DHA and GALD isomers are the first stable species to form upon $2e^-$ oxidation of one of the hydroxyl moieties of glycerol.[51,57] A higher yield of DHA compared to GALD (Fig. 3 and S19†) corroborates with DFT calculations that have identified DHA as the thermodynamically more stable product than GALD.[58] GCALD is proposed to form from isomeric DHA/GALD species through C–C bond cleavage, releasing one equivalent of FA. Subsequent C–C bond cleavage to form one more equivalent of FA and FMALD from GCALD is proposed as one of the further steps. The presence of hydrated GCALD was confirmed by HPLC and NMR spectroscopy (identification of its exact structure(s) in the solution, *i.e.* hydrated

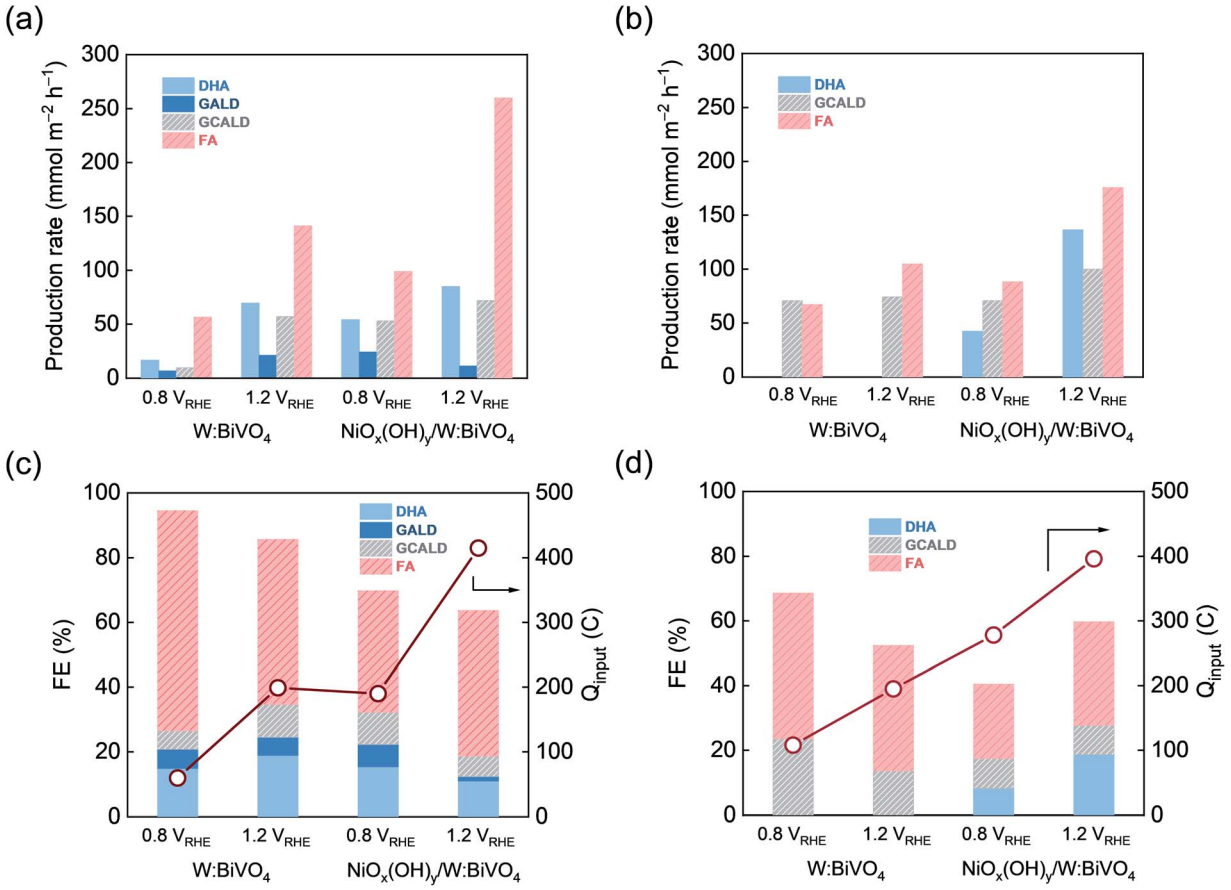

Fig. 3 Quantitative product analysis for different electrolytes after 10 h of continuous photoelectrolysis of 0.1 M glycerol solution over W:$BiVO_4$ and $NiO_x(OH)_y$/W:$BiVO_4$ electrodes at different applied voltages. Production rate (R, mmol m^{-2} h^{-1}) determined in (a) 0.5 M $Na_2SO_{4(aq)}$ and (b) 0.5 M KB_i; faradaic efficiency per mole of specific compound (FE, %; bars) and total charge transfer (Q_{input}, C; line) determined in (c) 0.5 M $Na_2SO_{4(aq)}$ and (d) 0.5 M KB_i using HPLC and ^{1}H NMR (DHA: dihydroxyacetone, GALD: glyceraldehyde, GCALD: glycolaldehyde dimers, and FA: formic acid or formate).

Table 1 Composition of products from 10 h photoelectrochemical glycerol oxidation (R: production rate, FE: faradaic efficiency)

Electrolyte	Electrode	Applied bias	Identified products[a]	Enhanced rate and FE of specific products observed with increased potential
Na_2SO_4	W:$BiVO_4$	0.8 V_{RHE}	GALD, DHA, GCALD, FA, FMALD	R_{DHA}, R_{GALD}, R_{GCALD}, R_{FA}, FE_{DHA}, FE_{GALD}, FE_{GCALD}
		1.2 V_{RHE}	GALD, DHA, GCALD, FA, FMALD	
	$NiO_x(OH)_y$/W:$BiVO_4$	0.8 V_{RHE}	GALD, DHA, GCALD, FA, FMALD	R_{DHA}, R_{GCALD}, R_{FA}
		1.2 V_{RHE}	GALD, DHA, GCALD, FA, FMALD	
KB_i	W:$BiVO_4$	0.8 V_{RHE}	GALD[b,d], GCALD, FA[b], FMALD[c]	R_{FA}
		1.2 V_{RHE}	GALD[b,d], GCALD, FA[b], FMALD[c]	
	$NiO_x(OH)_y$/W:$BiVO_4$	0.8 V_{RHE}	GALD[b,d], GCALD, DHA[b], FA[b], FMALD[c]	R_{DHA}, R_{GCALD}, R_{FA}, FE_{DHA}, FE_{FA}
		1.2 V_{RHE}	GALD[b,d], GCALD, DHA[b], FA[b], FMALD[c]	

[a] Reaction conditions: 0.1 M glycerol, electrode area 2.8 cm^2, volume of anode part 33 ml, temperature at 25 °C (DHA: dihydroxyacetone, GALD: glyceraldehyde, GCALD: glycolaldehyde dimers, FA: formate, and FMALD: formaldehyde). [b] Product that is identified by ^{1}H NMR only. [c] Product that is identified by ^{13}C NMR only, hence the quantitative analysis is not available. [d] Product that is identified by ^{1}H NMR; however, its chemical shifts overlap with GCALD.

monomers, dimers or oligomers,[59] is beyond the scope of this work).

In 0.5 M Na_2SO_4, PEC glycerol oxidation using a W:$BiVO_4$ electrode leads to higher amounts of GALD and GCALD at increased applied bias (1.2 V_{RHE} *vs.* 0.8 V_{RHE}). In contrast, $NiO_x(OH)_y$/W:$BiVO_4$ electrodes preferentially produce GALD and GCALD at a lower potential, 0.8 V_{RHE}, presumably due to their overoxidation at higher applied voltage. Although the deposition of a $NiO_x(OH)_y$ co-catalyst does not appear to alter the general reaction pathway, the presence of a nickel co-

catalyst strongly influences the product distribution (which is also affected by the applied bias and reaction media). For instance, $NiO_x(OH)_y$/W:$BiVO_4$ electrodes show an increased selectivity toward DHA formation over GCALD at 1.2 V_{RHE} in alkaline KB_i buffer. In contrast to a recent report, in which it was argued that the selective formation of DHA from glycerol is feasible,[60] our findings indicate that multiple products inevitably form upon glycerol photoelectrooxidation, emphasizing in turn the importance of the use of complementary analytical tools (*e.g.* HPLC and NMR spectroscopy) for an accurate quantitative analysis of the complex product mixture (see also Fig. S27†).

Conclusions

This study reveals key trends in the product distribution of the photoelectrochemical glycerol oxidation over $BiVO_4$-based electrodes in the presence/absence of a $NiO_x(OH)_y$ co-catalyst, at varying electrolyte environments. A quantitative product analysis was achieved by combining HPLC and ^{1}H NMR spectroscopy. We have found that GALD, DHA, GCALD, FA and FMALD are the primary products of glycerol oxidation. To the best of our knowledge, in this study GCALD was detected as a product of PEC glycerol oxidation for the first time. Importantly, we identify the conditions favouring the formation of the high value-added chemicals, DHA and GALD, thus providing a rare example of the system enabling production of valuable C_3 products from glycerol without the use of precious metal catalysts. We believe that the reported development of a system for the photoelectrochemical glycerol reforming relying on earth-abundant elements is an important step in the advancement of affordable solar-driven electrolyzers and direct alcohol fuel cells.

Conflicts of interest

There are no conflicts to declare.

Acknowledgements

We acknowledge Giovanni Bovone and Prof. Dr Mark Tibbitt for providing access to HPLC. We thank Prof. Dr Kristopher McNeill for providing access to the NMR spectrometer and for helpful discussions. Dr Sung Min Kim is acknowledged for assistance in the atomic layer deposition of the $NiO_x(OH)_y$ coatings. Dr Agnieszka Kierzkowska and Dr Felix Donat are thanked for ICP analysis. The work was supported by the Swiss Office of Energy (BFE, Grant Agreement No. SI/501598-01).

Notes and references

1 V. R. Stamenkovic, D. Strmcnik, P. P. Lopes and N. M. Markovic, *Nat. Mater.*, 2016, **16**, 57–69.
2 Z. W. Seh, J. Kibsgaard, C. F. Dickens, I. Chorkendorff, J. K. Nørskov and T. F. Jaramillo, *Science*, 2017, **355**, eaad4998.
3 I. Staffell, D. Scamman, A. Velazquez Abad, P. Balcombe, P. E. Dodds, P. Ekins, N. Shah and K. R. Ward, *Energy Environ. Sci.*, 2019, **12**, 463–491.
4 S. L. Foster, S. I. P. Bakovic, R. D. Duda, S. Maheshwari, R. D. Milton, S. D. Minteer, M. J. Janik, J. N. Renner and L. F. Greenlee, *Nat. Catal.*, 2018, **1**, 490–500.
5 J. G. Chen, R. M. Crooks, L. C. Seefeldt, K. L. Bren, R. M. Bullock, M. Y. Darensbourg, P. L. Holland, B. Hoffman, M. J. Janik, A. K. Jones, M. G. Kanatzidis, P. King, K. M. Lancaster, S. V. Lymar, P. Pfromm, W. F. Schneider and R. R. Schrock, *Science*, 2018, **360**, eaar6611.
6 M. D. Porosoff, B. Yan and J. G. Chen, *Energy Environ. Sci.*, 2016, **9**, 62–73.
7 A. Goeppert, M. Czaun, J.-P. Jones, G. K. Surya Prakash and G. A. Olah, *Chem. Soc. Rev.*, 2014, **43**, 7995–8048.
8 A. Tsoukalou, P. M. Abdala, D. Stoian, X. Huang, M. G. Willinger, A. Fedorov and C. R. Muller, *J. Am. Chem. Soc.*, 2019, **141**, 13497–13505.
9 S. J. Davis, N. S. Lewis, M. Shaner, S. Aggarwal, D. Arent, I. L. Azevedo, S. M. Benson, T. Bradley, J. Brouwer, Y.-M. Chiang, C. T. M. Clack, A. Cohen, S. Doig, J. Edmonds, P. Fennell, C. B. Field, B. Hannegan, B.-M. Hodge, M. I. Hoffert, E. Ingersoll, P. Jaramillo, K. S. Lackner, K. J. Mach, M. Mastrandrea, J. Ogden, P. F. Peterson, D. L. Sanchez, D. Sperling, J. Stagner, J. E. Trancik, C.-J. Yang and K. Caldeira, *Science*, 2018, **360**, eaas9793.
10 C. C. L. McCrory, S. Jung, I. M. Ferrer, S. M. Chatman, J. C. Peters and T. F. Jaramillo, *J. Am. Chem. Soc.*, 2015, **137**, 4347–4357.
11 J. H. Montoya, L. C. Seitz, P. Chakthranont, A. Vojvodic, T. F. Jaramillo and J. K. Norskov, *Nat. Mater.*, 2017, **16**, 70–81.
12 M. G. Walter, E. L. Warren, J. R. McKone, S. W. Boettcher, Q. Mi, E. A. Santori and N. S. Lewis, *Chem. Rev.*, 2010, **110**, 6446–6473.
13 D. W. Wakerley, M. F. Kuehnel, K. L. Orchard, K. H. Ly, T. E. Rosser and E. Reisner, *Nat. Energy*, 2017, **2**, 17021.
14 C. Mondelli, G. Gözaydın, N. Yan and J. Pérez-Ramírez, *Chem. Soc. Rev.*, 2020, **49**, 3764–3782.
15 P. R. d. l. Piscina and N. Homs, *Chem. Soc. Rev.*, 2008, **37**, 2459–2467.
16 M. Simões, S. Baranton and C. J. C. Coutanceau, *ChemSusChem*, 2012, **5**, 2106–2124.
17 D. G. Nocera, *Acc. Chem. Res.*, 2012, **45**, 767–776.
18 K. Sivula and R. van de Krol, *Nat. Rev. Mater.*, 2016, **1**, 15010.
19 A. Kudo, K. Omori and H. Kato, *J. Am. Chem. Soc.*, 1999, **121**, 11459–11467.
20 A. Kudo, K. Ueda, H. Kato and I. Mikami, *Catal. Lett.*, 1998, **53**, 229–230.
21 S. Tokunaga, H. Kato and A. Kudo, *Chem. Mater.*, 2001, **13**, 4624–4628.
22 S. J. A. Moniz, S. A. Shevlin, D. J. Martin, Z.-X. Guo and J. Tang, *Energy Environ. Sci.*, 2015, **8**, 731–759.
23 L. Zhang, D. Chen and X. Jiao, *J. Phys. Chem. B*, 2006, **110**, 2668–2673.

24 S. Gao, B. Gu, X. Jiao, Y. Sun, X. Zu, F. Yang, W. Zhu, C. Wang, Z. Feng and B. Ye, *J. Am. Chem. Soc.*, 2017, **139**, 3438–3445.
25 H. G. Cha and K.-S. Choi, *Nat. Chem.*, 2015, **7**, 328.
26 C.-H. Zhou, J. N. Beltramini, Y.-X. Fan and G. Q. Lu, *Chem. Soc. Rev.*, 2008, **37**, 527–549.
27 L. C. Meher, D. V. Sagar and S. N. Naik, *Renewable Sustainable Energy Rev.*, 2006, **10**, 248–268.
28 G. Dodekatos, S. Schünemann and H. Tüysüz, *ACS Catal.*, 2018, **8**, 6301–6333.
29 K. Zakaria, M. McKay, R. Thimmappa, M. Hasan, M. Mamlouk and K. Scott, *ChemElectroChem*, 2019, **6**, 2578–2585.
30 Z. Zhang, L. Xin, J. Qi, D. J. Chadderdon and W. Li, *Appl. Catal., B*, 2013, **136–137**, 29–39.
31 R. Subbaraman, D. Tripkovic, K.-C. Chang, D. Strmcnik, A. P. Paulikas, P. Hirunsit, M. Chan, J. Greeley, V. Stamenkovic and N. M. Markovic, *Nat. Mater.*, 2012, **11**, 550–557.
32 D. K. Bediako, Y. Surendranath and D. G. Nocera, *J. Am. Chem. Soc.*, 2013, **135**, 3662–3674.
33 V. L. Oliveira, C. Morais, K. Servat, T. W. Napporn, G. Tremiliosi-Filho and K. B. Kokoh, *J. Electroanal. Chem.*, 2013, **703**, 56–62.
34 X. Lu, S. Xie, H. Yang, Y. Tong and H. Ji, *Chem. Soc. Rev.*, 2014, **43**, 7581–7593.
35 K. J. McDonald and K.-S. Choi, *Energy Environ. Sci.*, 2012, **5**, 8553–8557.
36 D. K. Lee and K.-S. Choi, *Nat. Energy*, 2018, **3**, 53–60.
37 H. S. Park, K. E. Kweon, H. Ye, E. Paek, G. S. Hwang and A. J. Bard, *J. Phys. Chem. C*, 2011, **115**, 17870–17879.
38 A. S. Asundi, J. A. Raiford and S. F. Bent, *ACS Energy Lett.*, 2019, **4**, 908–925.
39 E. L. Ratcliff, J. Meyer, K. X. Steirer, A. Garcia, J. J. Berry, D. S. Ginley, D. C. Olson, A. Kahn and N. R. Armstrong, *Chem. Mater.*, 2011, **23**, 4988–5000.
40 K. A. Stoerzinger, W. T. Hong, X. R. Wang, R. R. Rao, S. B. Subramanyam, C. J. Li, Ariando, T. Venkatesan, Q. Liu, E. J. Crumlin, K. K. Varanasi and Y. Shao-Horn, *Chem. Mater.*, 2017, **29**, 9990–9997.
41 D. A. Kuznetsov, M. A. Naeem, P. V. Kumar, P. M. Abdala, A. Fedorov and C. R. Müller, *J. Am. Chem. Soc.*, 2020, **142**, 7883–7888.
42 L. Trotochaud, J. K. Ranney, K. N. Williams and S. W. Boettcher, *J. Am. Chem. Soc.*, 2012, **134**, 17253–17261.
43 M. Görlin, J. Ferreira de Araújo, H. Schmies, D. Bernsmeier, S. Dresp, M. Gliech, Z. Jusys, P. Chernev, R. Kraehnert, H. Dau and P. Strasser, *J. Am. Chem. Soc.*, 2017, **139**, 2070–2082.
44 D. A. Kuznetsov, J. Peng, L. Giordano, Y. Román-Leshkov and Y. Shao-Horn, *J. Phys. Chem. C*, 2020, **124**, 6562–6570.
45 A. Hagfeldt, H. Lindström, S. Södergren and S.-E. Lindquist, *J. Electroanal. Chem.*, 1995, **381**, 39–46.
46 C. Zachäus, F. F. Abdi, L. M. Peter and R. van de Krol, *Chem. Sci.*, 2017, **8**, 3712–3719.
47 T. W. Kim and K.-S. Choi, *Science*, 2014, **343**, 990–994.
48 F. M. Toma, J. K. Cooper, V. Kunzelmann, M. T. McDowell, J. Yu, D. M. Larson, N. J. Borys, C. Abelyan, J. W. Beeman, K. M. Yu, J. Yang, L. Chen, M. R. Shaner, J. Spurgeon, F. A. Houle, K. A. Persson and I. D. Sharp, *Nat. Commun.*, 2016, **7**, 12012.
49 N. S. Porter, H. Wu, Z. Quan and J. Fang, *Acc. Chem. Res.*, 2013, **46**, 1867–1877.
50 A. Villa, N. Dimitratos, C. E. Chan-Thaw, C. Hammond, L. Prati and G. J. Hutchings, *Acc. Chem. Res.*, 2015, **48**, 1403–1412.
51 C. Dai, L. Sun, H. Liao, B. Khezri, R. D. Webster, A. C. Fisher and Z. J. Xu, *J. Catal.*, 2017, **356**, 14–21.
52 T. Chatterjee, E. Boutin and M. Robert, *Dalton Trans.*, 2020, **49**, 4257–4265.
53 J. Kua, M. M. Galloway, K. D. Millage, J. E. Avila and D. O. De Haan, *J. Phys. Chem. A*, 2013, **117**, 2997–3008.
54 V. Waagen, T. K. Barua, H. W. Anthonsen, L. K. Hansen, D.-J. Fossli, E. Hough and T. Anthonsen, *Tetrahedron*, 1994, **50**, 10055–10060.
55 A. C. Garcia, Y. Y. Birdja, G. Tremiliosi-Filho and M. T. M. Koper, *J. Catal.*, 2017, **346**, 117–124.
56 S. Leukel, M. Mondeshki and W. Tremel, *Inorg. Chem.*, 2018, **57**, 11289–11298.
57 M. Simões, S. Baranton and C. Coutanceau, *Appl. Catal., B*, 2010, **93**, 354–362.
58 L. Cheng, C. Doubleday and R. Breslow, *Proc. Natl. Acad. Sci. U. S. A.*, 2015, **112**, 4218–4220.
59 V. A. Yaylayan, S. Harty-Majors and A. A. Ismail, *Carbohydr. Res.*, 1998, **309**, 31–38.
60 D. Liu, J. C. Liu, W. Cai, J. Ma, H. B. Yang, H. Xiao, J. Li, Y. Xiong, Y. Huang and B. Liu, *Nat. Commun.*, 2019, **10**, 1779.

